Role of Membrane Stretch in Adsorption of Antiviral Peptides onto Lipid Membranes and Membrane Pore Formation

Choon-Peng Chng[a], Nam-Joon Cho[b,c], K. Jimmy Hsia[a,d,*], and Changjin Huang[a,*]

[a] School of Mechanical and Aerospace Engineering, Nanyang Technological University, Singapore 639798, Republic of Singapore;

[b] School of Materials Science and Engineering, Nanyang Technological University, Singapore 637553, Republic of Singapore;

[c] China-Singapore International Joint Research Institute (CSIJRI), Guangzhou 510000, P.R. China;

[d] School of Chemical and Biomedical Engineering, Nanyang Technological University, Singapore 637459, Republic of Singapore.

[*] Corresponding authors: kjhsia@ntu.edu.sg and cjhuang@ntu.edu.sg

Abstract

Many medically important viruses are enveloped viruses, which are surrounded by a structurally conserved, host-derived lipid membrane coating. Agents that target and disrupt this membrane coating could potentially function as broad-spectrum antiviral drugs. The amphipathic α-helical (AH) peptide derived from the N-terminus of the hepatitis C virus NS5A protein is one such candidate and has been demonstrated to be able to selectively rupture lipid vesicles in the size range of viruses (< 160 nm diameter). However, the mechanism underlying this membrane curvature selectivity remains elusive. In this study, we have performed molecular dynamics simulations to study the binding of the AH peptide to model membranes that are stretched to resemble the looser lipid head-group packing present on highly curved outer membranes of nanoscale vesicles. We found that AH peptide binds more favorably to membranes that are stretched. In addition, a tetrameric placement of peptides across the membrane induced stable pore formation in the stretched membrane. Thus, our results suggest that AH peptide senses the high curvature of nanoscale vesicles via the enhanced exposure of lipid packing defects induced by membrane area strain.

Introduction

Many infectious diseases are caused by pathogenic viruses, such as flu by influenza virus, acquired immunodeficiency syndrome (AIDS) by human immunodeficiency virus, dengue fever by dengue virus, and the ongoing coronavirus disease 2019 (COVID-19) pandemic by severe acute respiratory syndrome coronavirus 2 (SARS-CoV-2). Existing antiviral drugs target either the viral replication machinery to stop viral genome replication within infected host cells, or the glycoproteins on the outer surface of viruses to hinder viral entry and/or release process.[1] Such strategies are prone to off-target errors and would fail to prevent the mutations leading to variant strains that are resistant to existing drugs. By contrast, the virus particle's lipid envelope is a structurally conserved component that is derived from the host cell membrane and helps the virus to avoid host immune response. In fact, most viruses causing epidemics are enveloped viruses, such as flaviviruses (e.g., dengue, yellow fever and zika) and coronaviruses (e.g., Middle East respiratory syndrome (MERS), SARS and COVID-19).[2] As the lipid envelope has a fluidic character, hosts surface glycoproteins that are necessary for virus entry and protects the viral genetic material, any change or disruption to the lipid envelope thus affects viral infectivity.[3]

Antiviral agents that target and disrupt the lipid envelope can potentially work as universal, broad-spectrum antiviral drugs against membrane-enveloped viruses.[4–6] For example, the amphipathic α-helical (AH) peptide derived from the N-terminus of the hepatitis C virus NS5A protein (Fig. 1(a)) has been identified as a promising antiviral peptide by targeting the virus particle's lipid envelope[7] and has demonstrated its therapeutic benefits *in vivo*.[8,9] The AH peptide was found to be able to completely rupture lipid vesicles with diameters smaller than 75 nm (according to quartz crystal microbalance-dissipation experiments), which is the size of many medically important enveloped viruses, such as hepatitis C virus, West Nile virus and flaviviruses.[10,11] The largest viruses that may be partially impaired by AH peptide are about 160 nm, which include the HIV and Measles viruses.[12] This size-selectivity is important as it would spare host cell membranes from possible toxic side effects. It has been discussed how the AH peptide preferentially forms pores in highly curved membranes, which leads to pore-induced membrane disruption.[13,14] However, the mechanism underlying membrane curvature-dependent binding and pore formation remains largely elusive so far, especially from a structural perspective.

It is known that many proteins can sense or induce large membrane curvatures.[15,16] Scaffold proteins, such as Bin/Amphiphysin/Rvs (BAR) domains, are intrinsically curved and bind to curved membranes via electrostatic interactions with the lipid head-groups.[16] Amphipathic helices feature a polar and an apolar face, and can sense lipid packing defects (loosely packed lipids exposing hydrophobic membrane core) via insertion of hydrophobic sidechains.[15,16] Examples of curvature-sensing peptides employing amphipathic helices include peptides with the ArfGAP1 lipid packing sensor (ALPS) motif,[17–21] MARCKS-ED,[22] TRP3,[23] and FAAV.[24] Although the proteins mentioned above involve specific structural features, it is now known that intrinsically disordered proteins (IDP) lacking a defined 3D structure could also function as potent membrane curvature sensors.[25,26] Curvature sensing by IDPs arises from an increase in conformational entropy (energetically favorable) on more highly curved membrane surfaces, with curvature sensitivity sharply increasing for vesicles less than 50 nm diameter.[25] In the case of peptides with amphipathic helices, ArfGAP1 is sensitive to vesicles smaller than 100 nm in diameter,[18] whereas MARCKS-ED shows a preference for vesicles as small as 30 nm diameter.[22] FAAV peptide showed enhanced binding to 50 nm diameter vesicles.[24] Since AH peptide contains both Phe and Trp residues and is sensitive to vesicles of similar size range, it might sense lipid packing defects as other amphipathic peptides do. Moreover, our recent study using coarse-grained molecular dynamics (MD) simulations found that a smaller nano-sized lipid vesicle features a higher membrane tension[27] and therefore the membranes of smaller vesicles are expected to be more stretched. The expected high membrane area strain in small vesicles is well correlated with the increase in the area/lipid and the decrease in lipid order observed in our simulations.[27] In a recent theoretical analysis, it was shown that, in very small vesicles with highly curved membranes, pores or even cup-shaped open vesicles may be stable configurations.[28] The facilitated formation of lipid packing defects on smaller vesicles in these studies is consistent with the more efficient pore formation and membrane destabilization observed experimentally for AH peptides, suggesting that membrane stretch plays an important role in regulating AH peptide-membrane interaction via regulating the exposure of packing defects.

In this study, we investigate the effects of mechanical deformation of lipid membrane – due to membrane curvature in different sized vesicles – on AH peptide-membrane

interaction. To understand the effects of membrane stretch on the AH peptide-membrane interaction, we simulate the interaction of AH peptides with a planar lipid membrane under increasing amounts of in-plane, bi-axial area strains (0%, 5%, 10%, and 20%) using all-atom MD simulations, illustrated as the “adsorption” step in Fig. 1(b). The increase in the lipid head-group separation in a stretched planar membrane resembles that on a curved membrane which is more technically challenging and/or computationally costly to simulate. All-atom MD simulations have been successfully conducted to characterize peptide-membrane interactions in past studies.[29–31] We find that the AH peptide tends to bind more strongly to the membrane as the membrane becomes stretched. Our simulations reveal the contributions of polar and positively charged residue sidechains to the binding of AH peptide on the stretched membrane surface, highlighting the importance of electrostatic interactions in AH peptide-membrane binding. Besides the initial binding, we also investigate the membrane disruptive effect of having single or four copies of AH peptides in a transmembrane conformation spanning across the membrane, illustrated as the “pore formation” step in Fig. 1(b). We find that four copies of AH peptides are able to generate and stabilize a water-filled membrane pore when the membrane is stretched, which is consistent with the suggested pore formation complex of four peptides from our previous work.[32] Our simulations also suggest that the flexible hinge in the helix-hinge-helix conformation of the AH peptide could play an important role in adapting the peptide’s transmembrane conformation to the change in the membrane thickness that is regulated by membrane stretch.

MD Simulations

Model of AH peptide in solution

The 3D structure of the AH peptide was predicted from amino acid sequence shown in Fig. 1(a) by the PEP-FOLD structure prediction server[33] and the highest ranked model (i.e. with the lowest energy) is taken as the initial model of AH peptide in solution. We performed MD simulation to refine this model using GROMACS version 2018.2 MD software.[34–36] The peptide was placed in a periodic cubic simulation box with 9 nm on each side and the simulation box was filled with TIP3P water molecules. The CHARMM27 force-field was used to describe inter-atomic interactions. Steepest descent energy minimization was first carried out for 5000 steps to remove any inter-

atomic steric clashes. Next, dynamics simulation was carried out with positional restraints on the protein atoms using canonical (NVT) ensemble for 100 ps at 300 K , followed by another 2 ns isobaric-isothermal (NPT) ensemble simulation at 300 K and 1 bar. Electrostatic interactions were computed using Particle Mesh Ewald method with cut-off distance of 1.0 nm. Van der Waals interactions were computed using cut-off method with cutoff distance of 1.0 nm. System temperature was maintained with the Velocity-rescale method with time constant of 0.1 ps, whereas pressure was maintained at 1 bar using the Berendsen method with time constant of 5 ps and compressibility of 4.5×10^{-5} bar^{-1}. Finally, restraints on the protein atoms were removed and simulation was carried out for 100 ns with temperature maintained at 300 K using the same method as above, but Parrinello-Rahman method was now used to control the pressure with a time constant of 2 ps and the same compressibility. The molecular structures in Fig. 1 and all subsequent figures were generated with Visual Molecular Dynamics (VMD) software v1.9.4.[37]

MD simulations of AH peptide-membrane interaction

The solution model obtained above was then used to study the binding of AH peptide to model membrane. As DOPC lipids were used to prepare lipid vesicles to study AH peptide activity in experiments,[38] a pre-equilibrated 256-lipid DOPC membrane was obtained from the CHARMM-GUI archive of pure lipid bilayers[39] to be used as the membrane model in this study. The CHARMM36 force-field was used for both peptide and DOPC membrane. The AH peptide was placed about 2 nm above the membrane with remaining space in the periodic simulation box filled with TIP3P water molecules. Energy minimization followed by MD simulations with restraints on protein and lipid head-group positions that were progressively reduced was carried out the relax the system. The unrestrained system was simulated for 30 ns with a time-step of 2 fs. Electrostatic interactions were computed using Particle Mesh Ewald method with cut-off distance of 1.2 nm. Van der Waals interactions were computed using cut-off method with forces smoothly switched to zero between 1.0 and 1.2 nm. System temperature was maintained at 303 K with the Nose-Hoover method with time constant of 1.0 ps, whereas pressure was maintained at 1 bar using the Parrinello-Rahman method with semi-isotropic coupling (X-Y plane coupled separately from the Z or bilayer normal direction) with time-constant of 5 ps and compressibility of 4.5×10^{-5}

bar^{-1}. Three independent simulations were carried out with different initial atomic velocities. The minimum distance between peptide atoms and membrane phosphate atoms was calculated using *mindist* program from GROMACS's suite of post-processing tools.

As peptide binding to the membrane surface is a stochastic event, to reduce the initial search process for the case of a stretched membrane, the peptide-bound configuration from one of the three independent simulations introduced above was used as the starting configuration for the stretched membrane. The planar membrane was stretched by simultaneously increasing the simulation box dimensions along the X and Y directions (membrane plane directions) at a rate of 0.0001 nm/ps until the desired membrane area strain (ratio of the change in membrane area to the initial membrane area) is achieved while maintaining the location of the bound peptide. To maintain the respective membrane area strain, simulations were performed using both NPT and NVT ensembles to reduce any possible bias due to the approach. For NPT ensembles, a specified pressure was maintained in the membrane plane which allowed the membrane area to fluctuate about the desired value under constant temperature (three independent simulations). For NVT ensembles, the membrane area fluctuated within a fixed simulation box under constant temperature (two independent simulations). Results from both approaches (total of five simulations) were combined and analyzed. The interaction energies (electrostatic + vdW) between peptide and lipid atoms were calculated using GROMACS post-processing tools.

Embedding AH peptides across DOPC membrane

An extended conformer of AH peptide sampled in the simulations was taken as the transmembrane model and embedded across the model DOPC membrane using the Membrane Builder tool within the CHARMM-GUI web-based platform.[39–42] The platform also provided optimal simulation protocol in setup files for GROMACS with the CHARMM36 force-field to describe peptide and membrane interactions.[43] The peptide(s) were oriented to span across the membrane. The membrane sizes were 9.5 nm × 9.5 nm with 256 DOPC lipids for the system with single peptide and 11 nm × 11 nm with 328 DOPC lipids for the system with four copies of the peptide. For the latter setup, the peptides were oriented such that polar/charged residue sidechains

were facing towards the center with hydrophobic sidechains facing out to the membrane lipids. The height of the periodic simulation box was 10 nm for both setups, with the space above and below the membrane filled with water molecules using the TIP3P water model.

After energy minimization steps, MD simulations were carried out with progressively reduced restraints on protein and lipid head-group positions as the simulation time-step was increased from 1 to 2 fs. Unrestrained simulations were then carried out for 60 ns (single peptide) or 50 ns (four copies of the peptide) to obtain the equilibrated configuration. Electrostatic and vdW interactions were handled in the same way as above for peptide-membrane interactions, as well as the temperature and pressure control methods. A constant strain was then applied in both the X and Y directions to stretch the simulation domain till the membrane area increased by about 20%. Simulations for another 60 ns (single peptide) or 50 ns (four copies of the peptide) were then conducted to obtain the new equilibrated configuration in the stretched membrane.

Results and Discussion

Simulation of AH peptide in water

The AH peptide contains multiple hydrophobic residues, including three Trp residues and one Phe residue. The 3D structure of the AH peptide was determined based on its amino acid sequence using the PEP-FOLD structure prediction server. The highest ranked model (with the lowest energy) is shown in Fig. 1(a). The predicted structure is U-shaped and consists of two helical segments joined by a hinge, featuring a so-called helix-turn-helix motif. The hydrophobic residue sidechains are mostly located in the region between the helices. Several positively charged sidechains (Lys and Arg) are present in the sequence and flank either side of the helices (shown as blue sticks in Fig. 1(a)). We performed MD simulations of the peptide in water for 100 ns and the equilibrated structure is shown in Fig. 1(a). Although no significant change to the secondary structure was observed (Fig. S1), a twist in the left helix containing Trp9 was observed to shift the Trp9 sidechain into the middle region and pack it against Trp22 on the right helix. The polar Lys26 sidechain, which was next to the hydrophobic Trp4 in the initial model and thus in an energetically unfavorable nonpolar environment,

now faces outwards to solvent, which is more energetically favorable as the Lys26 sidechain can now form hydrogen-bonds with water molecules. As a result, Trp4 now packs against Trp9. Together with Trp22, a hydrophobic core is formed which effectively reduces the exposure of these bulky hydrophobic sidechains to water (Fig. 1(a)). Hence, this equilibrated 3D structure is lower in energy and is expected to be a more stable conformation that AH peptide adopts in water. This solution structure of AH peptide was taken as the starting conformation to interrogate the role of membrane stretch in the peptide-membrane interaction during both the adsorption and pore formation steps (Fig. 1(b)).

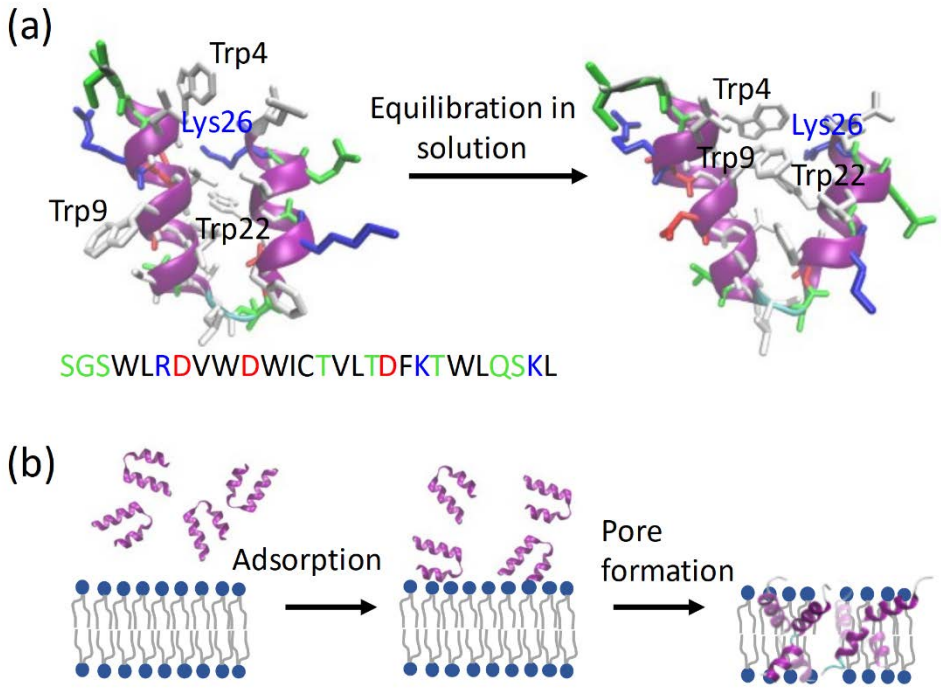

Figure 1. Structure of amphipathic α-helical (AH) peptide derived from the N-terminus of the hepatitis C virus NS5A protein and its mode of action on lipid membranes. (a) 3D structures of AH peptide predicted by the PEP-FOLD structure prediction server (*left*) and after 100 ns of MD simulations in water (*right*). Residue sidechains are colored according to residue type: blue for basic, red for acidic, green for polar and white for hydrophobic. The amino acid sequence of AH peptide is shown below the 3D structure and colored following the same scheme except that black is used for hydrophobic amino acids instead. (b) Schematic illustration of membrane binding and subsequent pore formation by AH peptides. The tetrameric arrangement of AH

peptides is taken from our current simulation. Membrane and peptides are not drawn to scale with orientation of peptides shown for illustration only.

Simulations of AH peptide adsorption on unstretched and stretched membranes

The AH peptide derived from the N-terminus of the hepatitis C virus NS5A protein was found to be able to selectively rupture lipid vesicles with diameters comparable to many medically important enveloped viruses (< 160 nm in diameter) and would thus spare host cell membranes from possible toxic side effects.[12] Our previous study on nanoscale lipid bilayer vesicles suggested that membrane tension increases as the size of vesicles decreases.[27] We have thus investigated the sensitivity of AH peptide to membrane stretch using all-atom MD simulations. The adsorption of AH peptide onto the membrane was studied using unbiased MD simulations, which allowed for free diffusion of the peptide in solution and on the phospholipid membrane surface, as illustrated in Fig. 1(b). The equilibrated AH peptide model in solution obtained above was placed about 2 nm above a DOPC phospholipid bilayer (Fig. 2(a)). Three replicate simulations were performed from the same starting configuration but with different sets of atomic velocities with the same mean determined by the system temperature to sample different diffusive behaviors. The minimum distance between the peptide and the phosphorous atoms in the lipid head-groups of the membrane was monitored as indications of peptide-membrane binding extent. Without membrane stretch, the simulations show that the AH peptide only transiently binds onto the membrane (min. distance < 0.5 nm), except for the first replicate in which stable binding (min. distance of 0.25 nm) was observed over about 5 ns before it rebounded (see black curve in Fig. 2(c)). In this replicate, the U-shaped peptide unfolded into a linear form. The other two replicates, however, remained U-shaped during the simulations. Overall, the simulations suggest that the AH peptide is not able to bind stably to the unstretched membrane. In marked contrast, on the stretched membrane (Fig. 2(b)), the AH peptide was observed to unbind and rebind onto the membrane surface in all three replicates (Fig. 2(d)). The peptide was able to remain bound stably for even up to 15 ns on the stretched membrane.

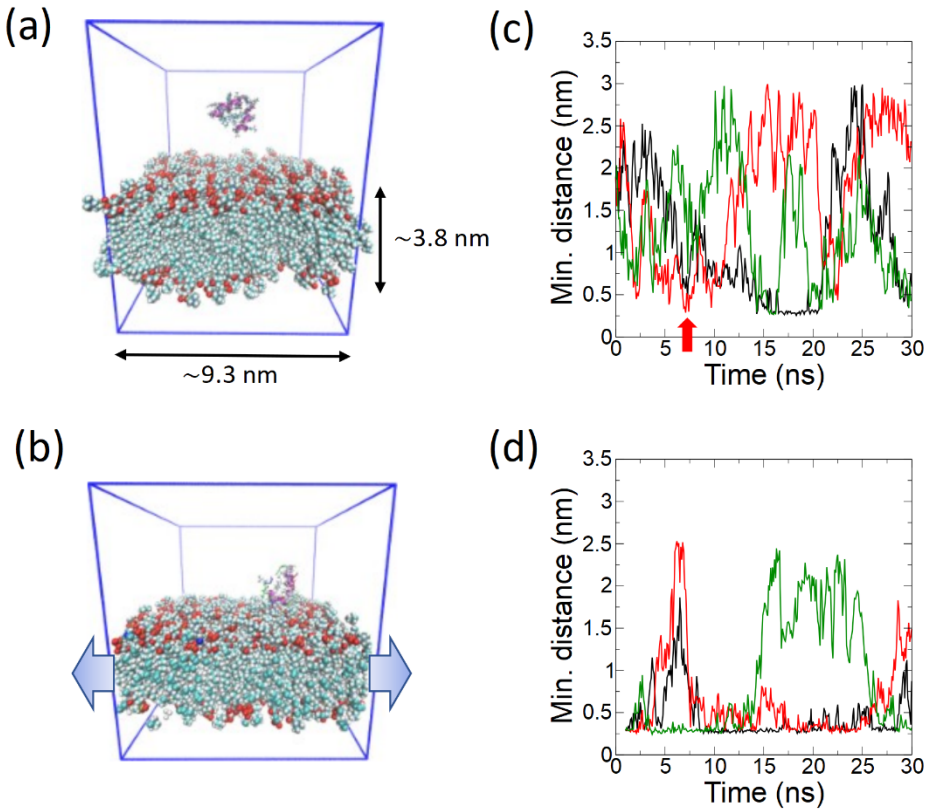

Figure 2. MD simulations of AH peptide on an either unstretched or stretched phospholipid membrane. (a) 3D computational model of an AH peptide placed above an unstretched DOPC membrane, with periodic boundaries in all coordinate directions and water omitted for clarity. (b) Computational model with a bound AH peptide on the membrane stretched by 10% of its initial area. (c-d) The temporal evolution of the minimum distance between AH peptide and phosphate atoms of the DOPC bilayer during three replicate simulations (black, red, and green traces, respectively) on the unstretched membrane (c) or the membrane stretched by 10% (d). Red arrow marks the starting configuration with bound AH for simulations under membrane stretch.

To understand the observed AH peptide-membrane binding behavior, we calculated and traced the total interaction energy between AH peptide and membrane (sum of electrostatic and van der Waals energies) as shown in Fig. S2. We can see that the interaction of AH peptide with the stretched membrane is stronger (more negative interaction energy) and more stable (longer lifetimes of bound state). This may be partially caused by the exposure of lipid packing defects with membrane tension which leads to more possible binding sites for AH peptide. From the time series, we have identified energetically favorable membrane-bound conformers on both unstretched

and stretched membranes (Fig. 3(a)). The conformers are labelled with subscript indicating the membrane area strain level and superscript labelling the order of the conformer starting with the one with the lowest binding energy. For example, C_{10}^{2} is the conformer with the second lowest binding energy at the membrane area strain of 10%. The peptide sidechains contributing to membrane binding are either polar (Ser, Thr and Trp) in nature, forming hydrogen bonds with membrane head-group phosphate oxygens, or positively charged (Lys and Arg), forming strong electrostatic attraction to the lipid head-group phosphate oxygens in addition to hydrogen bonds (electrostatic in nature). As the membrane is stretched, the membrane area per lipid increases, thus increasing the average phosphate-to-phosphate distance. This may have facilitated the peptide-membrane binding by making the phosphates more accessible to peptide sidechains. Ser1 was observed to contribute to the lowest energy conformers on both unstretched and stretched membranes due to its dual polar (sidechain) and positively charged (N atom on the N-terminal backbone) feature which allows it to form both hydrogen-bonds and electrostatic interactions with the membrane phosphates. Trp sidechain has both hydrophobic (aromatic ring) and polar (N-H group) nature, thus can potentially interact with the CH_3 groups on the lipid head-group as well as hydrogen-bond to membrane phosphates. The electrostatic interaction between the peptide and membrane lipid head-groups is thus the key driving force in the peptide-membrane binding event, with contributions by several polar and basic residue sidechains that might be tested in experiments.

The total interaction energy of the conformers becomes more negative as the membrane is stretched, implying stronger peptide-membrane binding (Fig. 3(b)). Among all the membrane-bound conformers identified in the unstretched membrane simulations, the linear AH peptide conformer has the lowest energy (labelled as C_{0}^{1} in Fig. 3(a)). However, its total interaction energy (−340 kJ/mol) is still higher than all of the top three lowest energy membrane-bound conformers identified in the stretched membrane simulations (Fig. 3(b)). More importantly, detailed analysis of the binding energy associated with individual sidechains reveals that, compared to the total interaction energy on the unstretched membrane, the same sidechain could lead to a much lower total interaction energy when interacting with the stretched membrane. For example, both C_{0}^{3} and C_{20}^{2} involve Lys20 and Thr17, but the magnitude of the total

interaction energy is nearly five-fold higher for C_{20}^2 suggesting the much stronger interaction between the sidechains and membrane phosphates (Fig. S3). This is possibly due to enhanced access to the phosphates on the stretched membrane. Note that ions are not included in our system because both AH peptide and DOPC lipids are charge neutral. In fact, we have confirmed that introducing ions into the system has little effect on AH peptide-membrane binding. As shown in Figure S4, both the peptide-membrane binding profile and the corresponding interaction energies in the system with sodium and chloride ions at a concentration of 0.15 M are similar to those obtained in the system without ions. We do not observe any strong binding of ions to the peptide. Although some sodium ions bind to the membrane phosphates, they do not seem to hinder peptide binding. The conformer with the lowest binding energy identified in the system with ions involves the same sidechains in C_{10}^1 in Fig. 3(a), but its total interaction energy (−450 kJ/mol) is less negative than that of C_{10}^1 (−600 kJ/mol). This again confirms that membrane stretch enhances AH peptide-membrane binding.

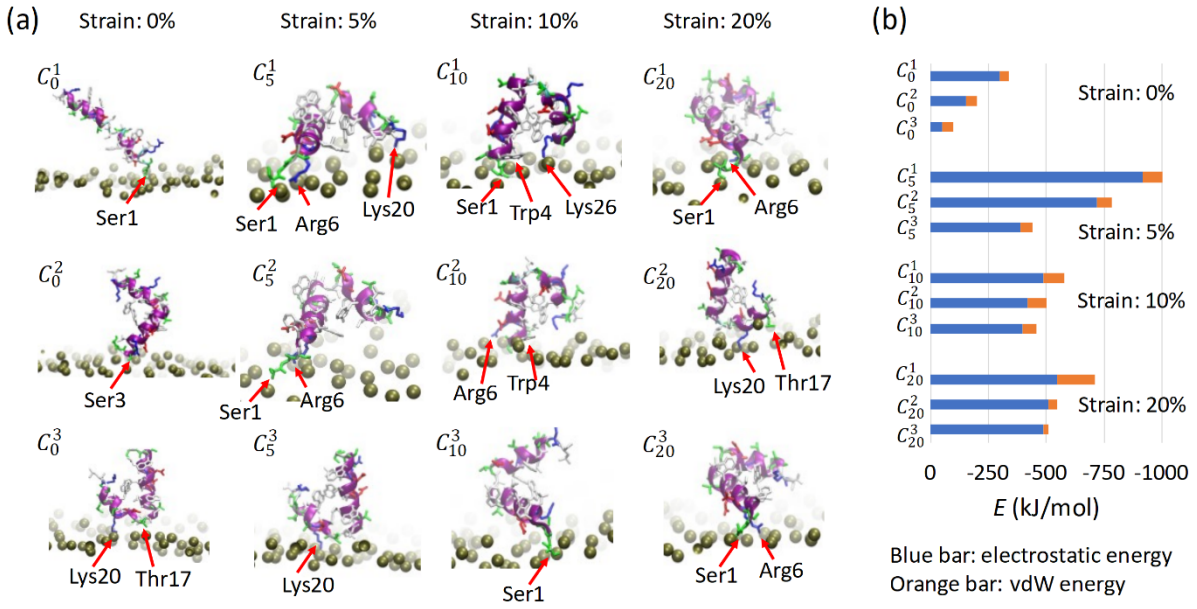

Figure 3. The snapshots and corresponding interaction energies of the low energy membrane-bound conformers on membranes under various stretch levels. (a) The top three lowest energy configurations of AH peptide under four different membrane area strain levels: 0%, 5%, 10% and 20%. (b) Bar plots of the corresponding interaction energies (electrostatic in blue and van der Waals in orange) between AH peptide and membrane for conformers in (a).

Previous all-atom MD simulations of a lipid transport protein with the ALPS motif also reported increased membrane binding on stretched 60:40 DOPC-DOPS membranes via increased exposure of lipid packing defects.[44] Furthermore, positively charged residues such as Lys was also found to contribute significantly to the peptide-membrane interaction energy in addition to bulky hydrophobic residues whereby Lys interacts with negatively charged phosphatidylserine head-group. Using liposomes ranging from 50-700 nm in diameter, previous experiments suggested that a higher density of binding sites via the exposure of lipid packing defects leads to enhanced binding of amphipathic motifs (which includes membrane-anchored proteins via alkyl chains) on highly curved membranes.[45] However, our analysis shows that membrane stretch not only exposes lipid packing defects, but also increases the binding affinity between AH peptide and the membrane. A higher binding affinity on curved membranes has also been reported for other amphipathic helices.[19,46] Although it has been found that AH peptide is capable to rupture lipid vesicles largely independently of the vesicle surface charge, the membrane surface charge strongly regulates the AH peptide-membrane interaction and consequently the kinetics of vesicle ruptue[47], which validates our finding of the importance of electrostatic interactions in AH peptide-membrane interaction.

Vesicle size sensitivity of AH peptide-induced rupture may be related to the degree of membrane stretch

Our finding of the enhanced binding affinity on stretched membranes sheds light on the vesicle size selectivity of AH peptide. As illustrated in Fig. 4(a), the smaller the vesicle, the higher membrane curvature and thus the higher the area strain in the outer leaflet of the vesicle membrane. Hence, although the packing geometry of the lipids in planar and curved membranes differ, the increased inter-lipid spacing on a stretched planar membrane is expected to resemble that on the convex side (the outer leaflet on a vesicle) of a curved membrane (Fig. 4(a)). The area strain in the stretched outer vesicle leaflet can be estimated as $\varepsilon_{out} = (a/a_0 - 1)$,[48] where a is the area/lipid of the outer vesicle leaflet and a_0 is the area/lipid of a tensionless planar bilayer composed of the same type of lipids. Based on the simple plate bending theory (see Supporting Information and Fig. S5), we can estimate the corresponding area strain in the outer leaflet of the vesicle membrane for a vesicle of a given size as $\varepsilon_{out} =$

$4r(D_{out} - r)/(D_{out} - 2r)^2$, where r is the radial distance of the neutral plane measured from the vesicle outer radius and D_{out} is the outer diameter of the vesicle, respectively. As shown in Table S1, the membrane area strain is predicted to increase with the reduction in vesicle size. Our previous MD simulations have revealed that the outer leaflet of a 24 nm diameter DMPC vesicle is under an area strain of about 20%, whereas the area strain increases to 31% for a 17 nm diameter DMPC vesicle.[27] These vesicle sizes are about 1.8× smaller than our estimates from the plate bending theory. Assuming that our highly simplified estimates are off by a factor of 1.8, this would suggest that a vesicle under 10% area strain would be about 46 nm in diameter. Hence, we argue that our stretched membranes in this study that are under 5%, 10% and 20% area strain correspond to vesicles of about 88 nm, 46 nm, and 24 nm in diameter, respectively. Note that the smallest DOPC vesicles used in previous investigations of membrane disruption by AH peptide is about 25 nm.[38]

Fig. 4(b) plots the peptide-membrane interaction energy (averaged over the top three lowest energies) as a function of the corresponding vesicle size with vesicles < 160 nm in diameter in the green (complete rupture) region, suggesting that the level of membrane area strain present in vesicles smaller than 160 nm could lead to enhanced AH peptide binding and thus vesicle rupture. The AH peptide-membrane interaction energy is expected to approach the energy level on a tensionless planar membrane when the vesicle size is sufficiently large. The limited power of AH peptide to rupture vesicles larger than 160 nm could be due to the much lower membrane area strain experienced by these vesicles (< 2.5% based on our rough estimates) which limits both the number of exposed lipid packing defects and the binding affinity between AH peptide and the vesicle.

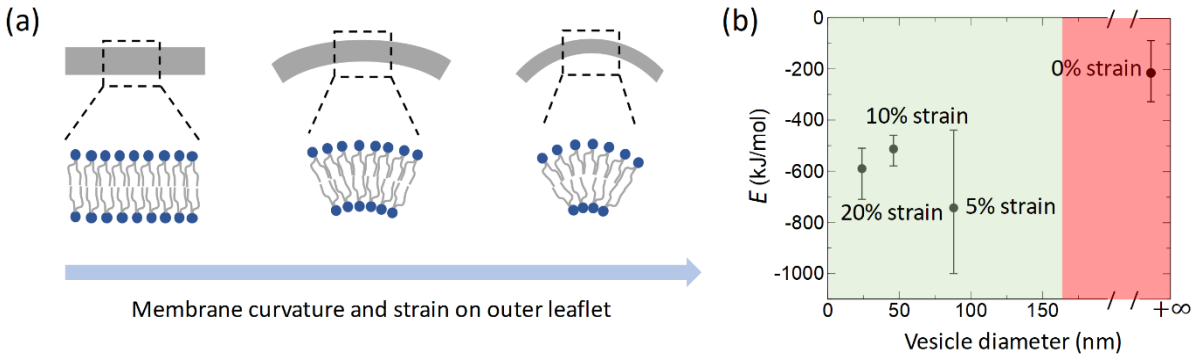

Figure 4. Proposed effect of vesicle size on AH peptide binding. (a) Schematic illustration of the lipid packing in flat, slightly curved, and highly curved membranes. As the lipid vesicle gets smaller, the membrane curvature increases and membrane area strain in the outer membrane leaflet also increases leading to increased exposure of lipid packing defects. (b) The values of the AH peptide-membrane interaction energies (average of the lowest three values shown as solid circles with error bars indicating the range) as a function of vesicle diameters, matched via the estimated membrane area strain levels. The data for the 0% area strain is matched to an infinitely large vesicle representing a flat membrane. The green region marks the vesicle size range within which complete rupture has been observed, whereas the red region (starting at 160 nm) is where vesicle rupture by AH peptide is not effective.

Simulations of membrane-embedded AH peptide(s) with and without membrane stretch

The ability of AH peptides to disrupt membranes has been attributed to their ability to induce pores on lipid vesicles in a curvature-dependent manner.[10,12,32] Our previous study has suggested that a nucleation pore can be formed by four AH peptides.[32] To reveal the molecular-level details on how AH peptides could induce pores in membranes, we have embedded either a single or four copies of AH peptides within a DOPC membrane using the CHARMM-GUI webserver. The extended conformer C_0^1 was adopted, as U-shaped conformers are too short to span the DOPC membrane. For a single AH peptide, the peptide configuration remains largely intact and tilts to accommodate the membrane thickness during both zero and 20% membrane area strain simulations (Fig. S6(a, c)). However, a thin water channel was observed in the stretched membrane but not in the unstretched one (Fig. S6(b, d)). The upper membrane leaflet was more significantly deformed under membrane area strain (indicated by the location of lipid head-group phosphate atoms), with a partially water-filled pore hydrating some of the polar peptide sidechains (Fig. S6(c, d)). This result suggests some degree of membrane destabilization even with a single peptide when the membrane is stretched.

For the four-peptide arrangement, we placed four copies of C_0^1 conformer in such a way that Lys20 sidechains were facing each other (Fig. 5(a)). After 50 ns, the initial

arrangement is slightly distorted with a bend forming at the hinge region of one of the peptides. The four peptides became less tightly packed, and no significant membrane distortion was observed. Although some water molecules were present in the membrane, they failed to form a continuous water channel (Fig. 5(b)). When the membrane is being stretched, all the peptides bend to different extents at their hinge regions (Fig. 5(c)). This could be driven by the membrane thinning effect under stretch.[21] Further simulations for 50 ns showed significant disturbance to the membrane as indicated by the head-group phosphate atoms. A stable water channel is observed (Fig. 5(d)). The top views of the tetrameric arrangements of AH peptides in the unstretched and stretched membrane after 50 ns of simulation are shown in Fig. 5(e-f), respectively. In the stretched membrane, the peptides become more loosely packed with a central pore and some of the helices became more horizontal, i.e., along the membrane-water interface (Fig. 5(f)). When visualizing the upper membrane as a surface, we could see clearly a pore lined by the peptides at 50 ns (Fig. 5(g)). The pore remained stable even after extending the simulation to 80 ns. Given that a stable pore is formed in a relatively short time-scale sub-100 ns in all-atom MD simulations, it confirms that membrane stretch facilitates the significant membrane disturbance caused by four AH peptides that together form a tetrameric pore.

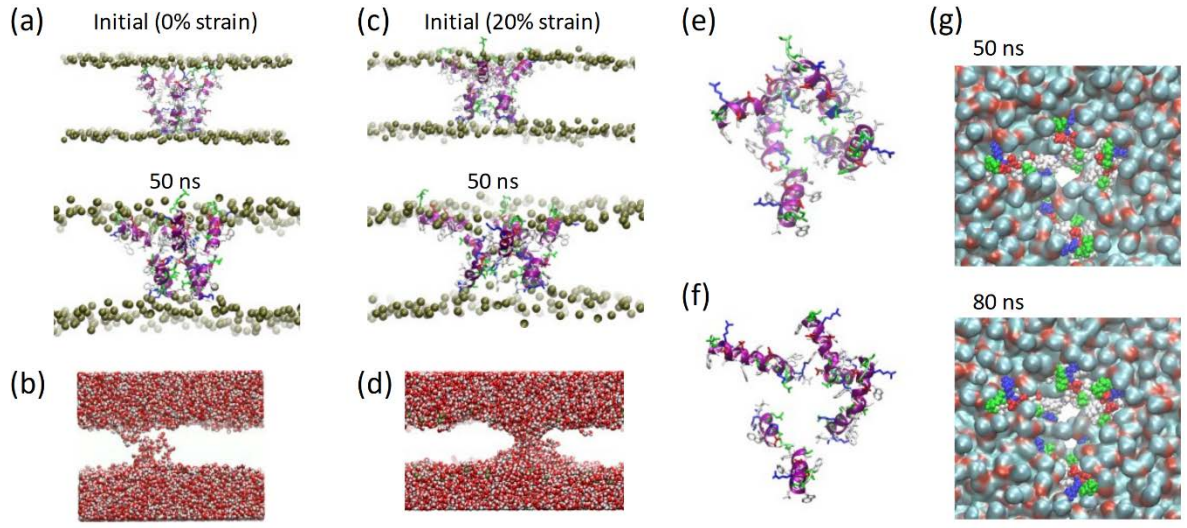

Figure 5. Membrane stretch-facilitated water pore formation by four copies of AH peptides. (a) Side views of the initial and equilibrated configurations of four copies of the C_0^1 AH conformer embedded in an unstretched DOPC membrane (peptide to lipid ratio of 4:328). Peptide sidechains (hydrogen atoms omitted) are shown as sticks with

colors following the same coloring scheme as in Fig. 1. (b) Side view of the configuration of water molecules at the end of the zero-area strain simulation. (c) Side views of the initial and equilibrated configurations of four copies of the C_0^1 AH conformer embedded in a DOPC membrane with its area stretched by 20%. (d) Side view of the configuration of water molecules at the end of the 20% strain simulation. (e-f) Top views of the tetrameric arrangement of AH peptides from the 50 ns snapshots in (a) and (c), respectively. (g) Top views of the membrane (shown as surface representation in VMD) with a pore surrounded by the four copies of AH peptides observed at 50 ns (same orientation as (f)) which remains present at 80 ns.

The pore formation might be facilitated by the reduced local elasticity of the membrane in the proximity of the AH peptides due to distortions to the lipid headgroups that are within the area enclosed by the peptides. The reduction in the local elasticity of the membrane is closely associated with the disruption to the packing order of the apolar lipid tails, which is similar to what we have found when -OOH groups are attached to lipid tails as a result of hydroperoxidation.[49] Increased bending at the hinge region was observed for some of the peptides to accommodate the reduction to membrane thickness upon stretching. On the other hand, a single peptide spanning the membrane remains mostly straight even within a membrane under the same amount of area strain. Our simulations suggest a cooperative effect among the peptides to change their conformation via bending at the hinge region to bring the polar/charged sidechains closer together in the apolar environment of the lipid bilayer core. The flexibility provided by the hinge region might allow the aggregate to maintain stable inter-peptide interaction over a range of membrane thicknesses present on nanoscale lipid vesicles of various sizes.

Conclusions

In this work, by performing atomistic MD simulations, we found that membrane stretch may enhance the adsorption and membrane pore formation propensity of antiviral AH peptides. This rationalizes our previous experimental observation of the size-dependent vesicle rupture by AH peptides. Nanoscale lipid vesicles have highly curved and stretched membranes which may facilitate exposure of lipid packing defects. Those lipid packing defects are sensed by AH peptide and other so-called curvature-

sensing peptides which do not possess membrane-lysing capability.[17–20,22–24] Hence, the exposure of lipid packing defects via membrane stretching, whether locally or globally on the outer membrane of a nanovesicle, may be a general mechanism to increase the adsorption (and hence clustering) and pore formation propensity of amphipathic peptides/molecules. The importance of specific basic and polar residues identified in this work to drive AH-membrane binding may be tested in future experiments. In addition, our simulations identified the important role of the flexible hinge of AH peptide in adapting the peptide's transmembrane conformation to the change in the membrane thickness during membrane pore formation process.

Supporting Information

Additional information is provided on how we estimate the area strain of the outer vesicle membrane from plate bending theory, Ramachandran plots showing secondary structural information about AH peptide before and after MD simulation (Figure S1), plots showing significant increase in electrostatic and vdW interaction energies between AH peptide and membrane with a 10% membrane area strain (Figure S2), plots showing how 20% membrane area strain significantly increases interaction of polar residue sidechains and membrane atoms (Figure S3), plots showing that addition of counterions have little impact on AH peptide-membrane interactions (Figure S4), schematic illustration of the stretching of the outer membrane leaflet that accompanies bending of a membrane patch (Figure S5), figures showing the slight membrane disturbance and transient membrane pore with a single AH peptide across the membrane under 20% membrane area strain (Figure S6), estimations of the vesicle outer diameters at a given membrane strain based on plate bending theory (Table S1), and estimations of the location of the neutral plane for DMPC vesicle membranes (Table S2).

Conflicts of interest

There are no conflicts to declare.

Acknowledgements

K.J.H. and C.H. acknowledge the financial support by the NIH Eunice Kennedy Shriver National Institute of Child Health and Human Development (grant R01HD086325). N-J.C. would like to acknowledge support from the China-Singapore International Joint

Research Institute (CSIJRI). K.J.H. would like to acknowledge financial support from Nanyang Technological University (start-up grant M4082428). C.H. would also like to acknowledge financial support from Nanyang Technological University (start-up grant M4082352) and the Ministry of Education, Singapore, under its Academic Research Fund Tier 1 (RG92/19). The computational work for this article was fully performed on resources of the National Supercomputing Centre, Singapore (https://www.nscc.sg).

References

(1) Jackman, J. A.; Yoon, B. K.; Ouyang, L.; Wang, N.; Ferhan, A. R.; Kim, J.; Majima, T.; Cho, N. J. Biomimetic Nanomaterial Strategies for Virus Targeting: Antiviral Therapies and Vaccines. *Adv. Funct. Mater.* **2021**, *31* (12), 1–25. https://doi.org/10.1002/adfm.202008352.

(2) Yoon, B. K.; Jeon, W. Y.; Sut, T. N.; Cho, N. J.; Jackman, J. A. Stopping Membrane-Enveloped Viruses with Nanotechnology Strategies: Toward Antiviral Drug Development and Pandemic Preparedness. *ACS Nano* **2021**, *15* (1), 125–148. https://doi.org/10.1021/acsnano.0c07489.

(3) Vigant, F.; Santos, N. C.; Lee, B. Broad-Spectrum Antivirals against Viral Fusion. *Nat. Rev. Microbiol.* **2015**, *13* (7), 426–437. https://doi.org/10.1038/nrmicro3475.

(4) Jackman, J. A.; Cho, N.-J. Targeting the Achilles Heel of Zika Virus and Other Emerging Viral Pathogens. *Adv. Ther.* **2018**, *1* (5), 1800045. https://doi.org/10.1002/adtp.201800045.

(5) Jackman, J. A.; Shi, P. Y.; Cho, N. J. Targeting the Achilles Heel of Mosquito-Borne Viruses for Antiviral Therapy. *ACS Infect. Dis.* **2019**, *5* (1), 4–8. https://doi.org/10.1021/acsinfecdis.8b00286.

(6) Cho, N. J.; Glenn, J. S. Materials Science Approaches in the Development of Broad-Spectrum Antiviral Therapies. *Nat. Mater.* **2020**, *19* (8), 810–820. https://doi.org/10.1038/s41563-020-0746-0.

(7) Cho, N. J.; Cho, S. J.; Kwang, H. C.; Glenn, J. S.; Frank, C. W. Employing an Amphipathic Viral Peptide to Create a Lipid Bilayer on Au and TiO2. *J. Am. Chem. Soc.* **2007**, *129* (33), 10050–10051. https://doi.org/10.1021/ja0701412.

(8) Jackman, J. A.; Costa, V. V.; Park, S.; Real, A. L. C. V.; Park, J. H.; Cardozo, P. L.; Ferhan, A. R.; Olmo, I. G.; Moreira, T. P.; Bambirra, J. L.; Queiroz, V. F.; Queiroz-Junior, C. M.; Foureaux, G.; Souza, D. G.; Ribeiro, F. M.; Yoon, B. K.; Wynendaele, E.; De Spiegeleer, B.; Teixeira, M. M.; Cho, N. J. Therapeutic Treatment of Zika Virus Infection Using a Brain-Penetrating Antiviral Peptide. *Nat. Mater.* **2018**, *17* (11), 971–977. https://doi.org/10.1038/s41563-018-0194-2.

(9) Camargos, V. N.; Foureaux, G.; Medeiros, D. C.; da Silveira, V. T.; Queiroz-Junior, C. M.; Matosinhos, A. L. B.; Figueiredo, A. F. A.; Sousa, C. D. F.; Moreira, T. P.; Queiroz, V. F.; Dias, A. C. F.; Santana, K. T. O.; Passos, I.; Real, A. L. C. V.; Silva, L. C.; Mourão, F. A. G.; Wnuk, N. T.; Oliveira, M. A. P.; Macari, S.; Silva, T.; Garlet, G. P.; Jackman, J. A.; Soriani, F. M.; Moraes, M. F. D.; Mendes, E. M. A. M.; Ribeiro, F. M.; Costa, G. M. J.; Teixeira, A. L.; Cho, N. J.; Oliveira, A. C. P.; Teixeira, M. M.; Costa, V. V.; Souza, D. G. In-Depth Characterization of Congenital Zika Syndrome in Immunocompetent Mice: Antibody-Dependent Enhancement and an Antiviral Peptide Therapy. *EBioMedicine* **2019**, *44*, 516–529. https://doi.org/10.1016/j.ebiom.2019.05.014.

(10) Cho, N. J.; Dvory-Sobol, H.; Xiong, A.; Cho, S. J.; Frank, C. W.; Glenn, J. S. Mechanism of an Amphipathic α-Helical Peptide's Antiviral Activity Involves Size-Dependent Virus Particle Lysis. *ACS Chem. Biol.* **2009**, *4* (12), 1061–1067. https://doi.org/10.1021/cb900149b.

(11) Jackman, J. A.; Cho, N. J. Model Membrane Platforms for Biomedicine: Case Study on Antiviral Drug Development. *Biointerphases* **2012**, *7* (1–4), 1–20. https://doi.org/10.1007/s13758-011-0018-2.

(12) Jackman, J. A.; Zan, G. H.; Zhdanov, V. P.; Cho, N. J. Rupture of Lipid Vesicles by a Broad-Spectrum Antiviral Peptide: Influence of Vesicle Size. *J. Phys. Chem. B* **2013**, *117* (50), 16117–16128. https://doi.org/10.1021/jp409716p.

(13) Tabaei, S. R.; Rabe, M.; Zhdanov, V. P.; Cho, N. J.; Höök, F. Single Vesicle Analysis Reveals Nanoscale Membrane Curvature Selective Pore Formation in Lipid Membranes by an Antiviral α-Helical Peptide. *Nano Lett.* **2012**, *12* (11), 5719–5725. https://doi.org/10.1021/nl3029637.

(14) Jackman, J. A.; Saravanan, R.; Zhang, Y.; Tabaei, S. R.; Cho, N. J. Correlation between Membrane Partitioning and Functional Activity in a Single Lipid Vesicle Assay Establishes Design Guidelines for Antiviral Peptides. *Small* **2015**, *11* (20), 2372–2379. https://doi.org/10.1002/smll.201403638.

(15) Bhatia, V. K.; Hatzakis, N. S.; Stamou, D. A Unifying Mechanism Accounts for Sensing of Membrane Curvature by BAR Domains, Amphipathic Helices and Membrane-Anchored Proteins. *Semin. Cell Dev. Biol.* **2010**, *21* (4), 381–390. https://doi.org/10.1016/j.semcdb.2009.12.004.

(16) Has, C.; Das, S. L. Recent Developments in Membrane Curvature Sensing and Induction by Proteins. *Biochim. Biophys. Acta - Gen. Subj.* **2021**, *1865* (10), 129971. https://doi.org/10.1016/j.bbagen.2021.129971.

(17) Bigay, J.; Gounon, P.; Roblneau, S.; Antonny, B. Lipid Packing Sensed by ArfGAP1 Couples COPI Coat Disassembly to Membrane Bilayer Curvature. *Nature* **2003**, *426*

(6966), 563–566. https://doi.org/10.1038/nature02108.

(18) Bigay, J.; Casella, J. F.; Drin, G.; Mesmin, B.; Antonny, B. ArfGAP1 Responds to Membrane Curvature through the Folding of a Lipid Packing Sensor Motif. *EMBO J.* **2005**, *24* (13), 2244–2253. https://doi.org/10.1038/sj.emboj.7600714.

(19) Drin, G.; Casella, J. F.; Gautier, R.; Boehmer, T.; Schwartz, T. U.; Antonny, B. A General Amphipathic α-Helical Motif for Sensing Membrane Curvature. *Nat. Struct. Mol. Biol.* **2007**, *14* (2), 138–146. https://doi.org/10.1038/nsmb1194.

(20) Wildermuth, K. D.; Monje-Galvan, V.; Warburton, L. M.; Klauda, J. B. Effect of Membrane Lipid Packing on Stable Binding of the ALPS Peptide. *J. Chem. Theory Comput.* **2019**, *15*, 1418–1429. https://doi.org/10.1021/acs.jctc.8b00945.

(21) van Hilten, N.; Stroh, K. S.; Risselada, H. J. Membrane Thinning Induces Sorting of Lipids and the Amphipathic Lipid Packing Sensor (ALPS) Protein Motif. *Front. Physiol.* **2020**, *11* (April), 250. https://doi.org/10.3389/fphys.2020.00250.

(22) Morton, L. A.; Yang, H.; Saludes, J. P.; Fiorini, Z.; Beninson, L.; Chapman, E. R.; Fleshner, M.; Xue, D.; Yin, H. MARCKS-ED Peptide as a Curvature and Lipid Sensor. *ACS Chem. Biol.* **2013**, *8* (1), 218–225. https://doi.org/10.1021/cb300429e.

(23) Bozelli, J. C.; Sasahara, E. T.; Pinto, M. R. S.; Nakaie, C. R.; Schreier, S. Effect of Head Group and Curvature on Binding of the Antimicrobial Peptide Tritrpticin to Lipid Membranes. *Chem. Phys. Lipids* **2012**, *165* (4), 365–373. https://doi.org/10.1016/j.chemphyslip.2011.12.005.

(24) Kawano, K.; Ogushi, M.; Masuda, T.; Futaki, S. Development of a Membrane Curvature-Sensing Peptide Based on a Structure – Activity Correlation Study. *Chem. Pharm. Bull.* **2019**, *67* (10), 1131–1138. https://doi.org/10.1248/cpb.c19-00465.

(25) Zeno, W. F.; Baul, U.; Snead, W. T.; DeGroot, A. C. M.; Wang, L.; Lafer, E. M.; Thirumalai, D.; Stachowiak, J. C. Synergy between Intrinsically Disordered Domains and Structured Proteins Amplifies Membrane Curvature Sensing. *Nat. Commun.* **2018**, *9* (1). https://doi.org/10.1038/s41467-018-06532-3.

(26) Zeno, W. F.; Thatte, A. S.; Wang, L.; Snead, W. T.; Lafer, E. M.; Stachowiak, J. C. Molecular Mechanisms of Membrane Curvature Sensing by a Disordered Protein. *J. Am. Chem. Soc.* **2019**, *141* (26), 10361–10371. https://doi.org/10.1021/jacs.9b03927.

(27) Chng, C. P.; Sadovsky, Y.; Hsia, K. J.; Huang, C. Curvature-Regulated Lipid Membrane Softening of Nano-Vesicles. *Extrem. Mech. Lett.* **2021**, *43*, 101174. https://doi.org/10.1016/j.eml.2021.101174.

(28) Huang, C.; Quinn, D.; Sadovsky, Y.; Suresh, S.; Hsia, K. J. Formation and Size Distribution of Self-Assembled Vesicles. *Proc. Natl. Acad. Sci.* **2017**, *114* (11), 2910–2915. https://doi.org/10.1073/pnas.1702065114.

(29) Huang, K.; García, A. E. Free Energy of Translocating an Arginine-Rich Cell-

Penetrating Peptide across a Lipid Bilayer Suggests Pore Formation. *Biophys. J.* **2013**, *104* (2), 412–420. https://doi.org/10.1016/j.bpj.2012.10.027.

(30) Irudayam, S. J.; Berkowitz, M. L. Binding and Reorientation of Melittin in a POPC Bilayer: Computer Simulations. *Biochim. Biophys. Acta - Biomembr.* **2012**, *1818* (12), 2975–2981. https://doi.org/10.1016/j.bbamem.2012.07.026.

(31) Perrin, B. S.; Pastor, R. W. Simulations of Membrane-Disrupting Peptides I: Alamethicin Pore Stability and Spontaneous Insertion. *Biophys. J.* **2016**, *111* (6), 1248–1257. https://doi.org/10.1016/j.bpj.2016.08.014.

(32) Jackman, J. A.; Goh, H. Z.; Zhdanov, V. P.; Knoll, W.; Cho, N. J. Deciphering How Pore Formation Causes Strain-Induced Membrane Lysis of Lipid Vesicles. *J. Am. Chem. Soc.* **2016**, *138* (4), 1406–1413. https://doi.org/10.1021/jacs.5b12491.

(33) Shen, Y.; Maupetit, J.; Derreumaux, P.; Tufféry, P. Improved PEP-FOLD Approach for Peptide and Miniprotein Structure Prediction. *J. Chem. Theory Comput.* **2014**, *10* (10), 4745–4758. https://doi.org/10.1021/ct500592m.

(34) Abraham, M. J.; Murtola, T.; Schulz, R.; Páll, S.; Smith, J. C.; Hess, B.; Lindahl, E. GROMACS: High Performance Molecular Simulations through Multi-Level Parallelism from Laptops to Supercomputers. *SoftwareX* **2015**, *1*, 19–25. https://doi.org/10.1016/j.softx.2015.06.001.

(35) Páll, S.; Abraham, M. J.; Kutzner, C.; Hess, B.; Lindahl, E. Tackling Exascale Software Challenges in Molecular Dynamics Simulations with GROMACS. In *Solving software challenges for exascale*; Markidis, S., Laure, E., Eds.; Springer, Cham, 2015; pp 3–27. https://doi.org/10.1007/978-3-319-15976-8_1.

(36) Pronk, S.; Páll, S.; Schulz, R.; Larsson, P.; Bjelkmar, P.; Apostolov, R.; Shirts, M. R.; Smith, J. C.; Kasson, P. M.; van der Spoel, D.; Hess, B.; Lindahl, E. GROMACS 4.5: A High-Throughput and Highly Parallel Open Source Molecular Simulation Toolkit. *Bioinformatics* **2013**, *29*, 845–854. https://doi.org/10.1093/bioinformatics/btt055.

(37) Humphrey, W.; Dalke, A.; Schulten, K. VMD: Visual Molecular Dynamics. *J. Mol. Graph.* **1996**, *14* (1), 33–38. https://doi.org/10.1016/0263-7855(96)00018-5.

(38) Park, S.; Jackman, J. A.; Cho, N. J. Comparing the Membrane-Interaction Profiles of Two Antiviral Peptides: Insights into Structure-Function Relationship. *Langmuir* **2019**, *35* (30), 9934–9943. https://doi.org/10.1021/acs.langmuir.9b01052.

(39) Jo, S.; Kim, T.; Im, W. Automated Builder and Database of Protein/Membrane Complexes for Molecular Dynamics Simulations. *PLoS One* **2007**, *2* (9), e880. https://doi.org/10.1371/journal.pone.0000880.

(40) Jo, S.; Kim, T.; Iyer, V. G.; Im, W. CHARMM-GUI: A Web-Based Graphical User Interface for CHARMM. *J. Comput. Chem.* **2008**, *29*, 1859–1865. https://doi.org/10.1002/jcc.20945.

(41) Jo, S.; Lim, J. B.; Klauda, J. B.; Im, W. CHARMM-GUI Membrane Builder for Mixed Bilayers and Its Application to Yeast Membranes. *Biophys. J.* **2009**, *97* (1), 50–58. https://doi.org/10.1016/j.bpj.2009.04.013.

(42) Wu, E. L.; Cheng, X.; Jo, S.; Rui, H.; Song, K. C.; Dávila-Contreras, E. M.; Qi, Y.; Lee, J.; Monje-Galvan, V.; Venable, R. M.; Klauda, J. B.; Im, W. CHARMM-GUI Membrane Builder toward Realistic Biological Membrane Simulations. *J. Comput. Chem.* **2014**, *35* (27), 1997–2004. https://doi.org/10.1002/jcc.23702.

(43) Lee, J.; Cheng, X.; Swails, J. M.; Yeom, M. S.; Eastman, P. K.; Lemkul, J. A.; Wei, S.; Buckner, J.; Jeong, J. C.; Qi, Y.; Jo, S.; Pande, V. S.; Case, D. A.; Brooks, C. L.; MacKerell, A. D.; Klauda, J. B.; Im, W. CHARMM-GUI Input Generator for NAMD, GROMACS, AMBER, OpenMM, and CHARMM/OpenMM Simulations Using the CHARMM36 Additive Force Field. *J. Chem. Theory Comput.* **2016**, *12* (1), 405–413. https://doi.org/10.1021/acs.jctc.5b00935.

(44) Monje-Galvan, V.; Klauda, J. B. Preferred Binding Mechanism of Osh4's Amphipathic Lipid-Packing Sensor Motif, Insights from Molecular Dynamics. *J. Phys. Chem. B* **2018**, *122* (42), 9713–9723. https://doi.org/10.1021/acs.jpcb.8b07067.

(45) Hatzakis, N. S.; Bhatia, V. K.; Larsen, J.; Madsen, K. L.; Bolinger, P. Y.; Kunding, A. H.; Castillo, J.; Gether, U.; Hedegård, P.; Stamou, D. How Curved Membranes Recruit Amphipathic Helices and Protein Anchoring Motifs. *Nat. Chem. Biol.* **2009**, *5* (11), 835–841. https://doi.org/10.1038/nchembio.213.

(46) Nuscher, B.; Kamp, F.; Mehnert, T.; Odoy, S.; Haass, C.; Kahle, P. J.; Beyer, K. α-Synuclein Has a High Affinity for Packing Defects in a Bilayer Membrane: A Thermodynamics Study. *J. Biol. Chem.* **2004**, *279* (21), 21966–21975. https://doi.org/10.1074/jbc.M401076200.

(47) Zan, G. H.; Jackman, J. A.; Cho, N. J. AH Peptide-Mediated Formation of Charged Planar Lipid Bilayers. *J. Phys. Chem. B* **2014**, *118* (13), 3616–3621. https://doi.org/10.1021/jp411648s.

(48) Miao, L.; Seifert, U.; Wortis, M.; Dobereinert, H. Budding Transitions of Fluid-Bilayer Vesicles: The Effect of Area-Difference Elasticity. *Phys. Rev. E* **1994**, *49* (6), 5389–5407.

(49) Chng, C.; Sadovsky, Y.; Hsia, K. J.; Huang, C. Site-Specific Peroxidation Modulates Lipid Bilayer Mechanics. *Extrem. Mech. Lett.* **2021**, *42*, 101148. https://doi.org/10.1016/j.eml.2020.101148.

For Table of Contents Only